sustainability

MDPI

Article

Optimization, Characterization, and Biological Applications of Silver Nanoparticles Synthesized Using Essential Oil of Aerial Part of *Laggera tomentosa*

Yilma Hunde Gonfa [1,2], Abiy Abebe Gelagle [3], Bekele Hailegnaw [4], Samuel Abicho Kabeto [1,2], Getachew Adam Workeneh [1,2], Fekade Beshah Tessema [1,2], Mesfin Getachew Tadesse [1,2], Saikh M. Wabaidur [5], Kholood A. Dahlous [5], Sami Abou Fayssal [6,7], Pankaj Kumar [8], Bashir Adelodun [9,10], Archana Bachheti [11] and Rakesh Kumar Bachheti [1,2,*]

1 Department of Industrial Chemistry, College of Applied Sciences, Addis Ababa Science and Technology University, Addis Ababa P.O. Box 16417, Ethiopia
2 Nanotechnology Centre of Excellence, Addis Ababa Science and Technology University, Addis Ababa P.O. Box 16417, Ethiopia
3 Ethiopian Public Health Institute, Addis Ababa P.O. Box 1242, Ethiopia
4 Institute of Physical Chemistry and Linz Institute for Organic Solar Cells, Johannes Kepeler University, 4040 Linz, Austria
5 Department of Chemistry, College of Science, King Saud University, Riyadh 11451, Saudi Arabia
6 Department of Agronomy, Faculty of Agronomy, University of Forestry, 10 Kliment Ohridski Blvd, 1797 Sofia, Bulgaria
7 Department of Plant Production, Faculty of Agriculture, Lebanese University, Beirut 1302, Lebanon
8 Agro-ecology and Pollution Research Laboratory, Department of Zoology and Environmental Science, Gurukula Kangri (Deemed to Be University), Haridwar 249404, India
9 Department of Agricultural and Biosystems Engineering, University of Ilorin, Ilorin 240003, Nigeria
10 Department of Agricultural Civil Engineering, Kyungpook National University, Daegu 41566, Republic of Korea
11 Department of Environment Science, Graphic Era University, Dehradun 248002, India
* Correspondence: rkbachheti@gmail.com or rakesh.kumar@aastu.edu.et

Abstract: Biological synthesis of silver nanoparticles (AgNPs) is a green, simple, cost-effective, time-efficient, and single-step method. This study mainly focused on the synthesis of silver nanoparticles (AgNPs) using essential oil of *Laggera tomentosa* (LTEO) and investigates their potential applications. Ultraviolet-Visible (UV-Vis) result showed the characteristic Surface Plasmon Resonance (SPR) peak of LTEO-AgNPs at 420 nm. Fourier transform infrared (FT-IR) spectroscopy indicated the functional groups present in LTEO and LTEO-AgNPs. Scanning electron microscope (SEM) image depicted the synthesized AgNPs mainly has spherical shapes with average nanoparticles size 89.59 ± 5.14 nm. Energy dispersive X-ray (EDX) peak at 3.0 keV showed the presence of Ag element in LTEO-AgNPs. The X-ray diffraction (XRD) peaks at 38°, 44° and 67° are assigned to (111), (200), and (220), respectively which displays the crystal nature of LTEO-AgNPs. The average particle size and zeta potential of LTEO-AgNPs were determined as 94.98 nm and −49.6 mV, respectively. LTEO-AgNPs were stable for six months against aggregation at room temperature. LTEO-AgNPs solutions exhibited potential activities for the treatment of some pathogenic bacteria species, agricultural productivity growth, determination of metallic ions, and catalytic reduction. This study is the first work to report nanoparticles synthesis using *L. tomentosa* extracts and evaluate their potential applications.

Keywords: phytochemicals; green nanoparticles; medicinal plants; AgNPs; biological applications

check for updates

Citation: Gonfa, Y.H.; Gelagle, A.A.; Hailegnaw, B.; Kabeto, S.A.; Workeneh, G.A.; Tessema, F.B.; Tadesse, M.G.; Wabaidur, S.M.; Dahlous, K.A.; Abou Fayssal, S.; et al. Optimization, Characterization, and Biological Applications of Silver Nanoparticles Synthesized Using Essential Oil of Aerial Part of *Laggera tomentosa*. *Sustainability* **2023**, *15*, 797. https://doi.org/10.3390/su15010797

Academic Editors: Sekar Vijayakumar, Roberto Christ Vianna Santos and Ramanathan Srinivasan

Received: 26 November 2022
Revised: 18 December 2022
Accepted: 26 December 2022
Published: 1 January 2023

1. Introduction

Green nanoparticles synthesis technology attracts the attention of many researchers over the last decades because of its eco-friendly, low cost, low energy, and single-step approach [1]. Nanoparticles (NPs) are reported with the unique average sizes less than 100 nm

and superior properties [2]. Noble metal nanoparticles (MNPs) showed extraordinary physical, chemical, and biological properties in various field of applications [3]. The biological methods of MNPs synthesis have greater advantages of application than the chemical and physical syntheses methods due to the toxicity problems of the latter approaches over the former one [4]. Plants are used as dominant sources of natural products for the synthesis of MNPs due to their biosafety and sustainability nature than other biological systems [5]. Optimization of the effects of various reaction parameters for the synthesis of MNPs plays a greater role in improving their properties and efficiency of applications [6]. High definite surface area and fraction of surface atom are the potential characteristics properties of MNPs for their broad range of applications [7].

Silver nanoparticles (AgNPs) synthesis is one of the vital research areas for the biological, medical, environmental, agricultural, and other applications because of the biocompatibility properties of biogenic NPs [8]. Plant extracts-mediated approach is the primary system for the biogenic synthesis of AgNPs [9]. Some previous studies revealed that essential oils are the potential candidate for the bioreduction of Ag^{+} ions to Ag^{0} during AgNPs formation [10]. Besides, the chemical components of essential oils act as the capping and stabilizing agents in the synthesized AgNPs [11,12]. Earlier research findings showed that antimicrobial, biomedical, colorimetric determination of metal ions, agriculture productivity growth, textile industry, catalytic reduction, and water treatment are some of the application areas of green AgNPs [12–14]. Currently, plants mediated AgNPs remain one of the hot research areas with remarkable biological and chemical applications [15]. Plants are considered as sustainable sources of bioreductants for the synthesis of AgNPs [16]. For example, capping of phytochemicals from essential oils of plants possesses the potential stabilizing properties in the formation of AgNPs [17]. The wide beneficial activities of essential oils in different areas of applications increase their interest of usage as bioreductants in the synthesis of AgNPs [18].

Plants' ecology, parts, age, season of collection, and method of extraction limit the diversity of chemical constituents of essential oils. Essential oils are mostly isolated from the leaves, stems, flowers, herbs, brushes, and aerial part of plant using the simple and inexpensive process such as distillation methods [19]. Hydrodistillation technique is often used to isolate essential oils from various parts of plants. This technique is usually favored for the isolation of essential oils due to its conventional, simplicity, low cost, greenness, and sustainable approach [20]. Essential oils were reported as complex mixtures of oxygenated and non-oxygenated hydrocarbons containing monoterpene, sesquiterpene, and other hydrocarbons [21,22]. Therefore, the diversified chemical compounds and functional groups of essential oils are responsible for the successful synthesis of AgNPs as potential bioreducing, capping, and stabilizing agents [23]. Aromatic plants are frequently used for different applications because of their potential source of essential oils [24]. The genus *Laggera* contains over 20 species which are mainly distributed in different ecological regions such as tropical Africa and Southeast Asia and known for their characteristic odor essences [25,26].

L. tomentosa Sch. Bip. Ex. Oliv. et Heirn (family of *Asteraceae*) is a known family of vascular herbs. It is a bushy perennial aromatic medicinal plant endemic to Ethiopia and is locally known as "Keskese" [27]. Different parts of the plant are traditionally used to treat toothache, stomachache, headache, swelling, and ringworm. Locally, the aerial part of the plant is also applied for cleansing milk containers and used as a fumigant [28]. In this regard, the plant species and its products can be used as the promising green agents for the treatment of food spoilage bacterial strains such as *Staphylococcus aureus*, *Staphylococcus epidermidis*, *Streptococcus agalactiae*, *Escherichia coli*, *Proteus mirabilis*, and *Pseudomonas aeruginosa* [29].

The essential oils of some *Laggera* species were reported for their potential applications as antimicrobial, antioxidant, larvicidal, and insecticidal agents [30]. Essential oil of *L. tomentosa* was reported to contain mainly monoterpenes and sesquiterpenes [28]. Even though the plant species is rich in natural products containing diversified bioactive components,

only little research work has been reported regarding their biological applications [30]. To the best of our knowledge, currently there is no published research report on the *L. tomentosa* extracts which mediated the synthesis of AgNPs and the study of their potential applications. Hence, the aim of this research is first to isolate essential oil from the aerial part of *L. tomentosa* (LTEO) and determine its phytochemical components. Then, apply the isolated LTEO for the green synthesis of AgNPs using the one factor at a time method of optimization of reaction conditions. Finally, potential activities of LTEO-AgNPs were evaluated using some pathogenic bacteria species, wheat seed germination and seedling growth, colorimetric determination of metal ions and catalytic reduction of *p*-nitrophenol to *p*-aminophenol as areas of applications.

2. Materials and Methods

2.1. Plant Material and Chemicals

L. tomentosa plant sample was collected from Tullu Dimtu, Addis Ababa Science and Technolgy University, Ethiopia, which is located at the latitude of 8°88′ N and longitude of 38°80′ E and elevation 2143 m above sea level (m.a.s.l.), in November 2020. Plant sample was collected and prepared according to the previously reported procedure by Asfaw et al. [29]. The aerial part of the plant sample was carefully cleaned and dried using the shading technique for 3 weeks. A dried sample of the plant was grinded to fine powder using the electric grinder and stored in a brown glass bottle until further analysis. In this study, all chemicals of analytical grade from Sigma-Aldrich (St. Louis, MO, USA) were used in all experiments. All the solutions were prepared using distilled water throughout the experiments.

2.2. Isolation and Characterization of Essential Oils

The procedure of isolation and characterization of essential oil was based on the earlier literature review [30]. The powder of dried sample (3 kg) was subjected to hydrodistillation in a Clevenger-type apparatus for 3 h. Then, the isolated *L. tomentosa* essential oil (LTEO) was dried over anhydrous Na_2SO_4 from the aqueous phase. Finally, LTEO was stored in the refrigerator until the further analysis. The percentage yield of isolated LTEO was determined and expressed as the ratio of isolated EO in millimeter unit to the weight of the plant sample used (dry weight) in 100 g (%*v*/*w*). The density, refractive index, and optical rotation of LTEO were determined by using a density meter (A. Kruss Optronic, Hamburg, Germany), refractometer (A. Kruss Optronic, Hamburg, Germany), and optical spectrometer (ADP600 series, Bellingham plus Stanley, Royal Tunbridge Wells, UK), respectively. The chemical composition determination of LTEO was carried out by the gas chromatography-mass spectrometry (GC-MS) (Thermo Fisher Scientific Inc., Waltham, MA, USA) technique. The analysis was performed according to the previous report procedure [22] with some manor modifications. A Varian CP-3800 gas-chromatograph equipped with a DB-capillary column (30 m × 0.25 mm coating thickness 0.25 µm) and a Varian Saturn 2000 ion trap mass detector was used for the sample analysis. The identification of chemical components of LTEO was performed by comparing their retention times with those of authentic samples and linear Kovat's indices with the series of n-alkanes (C_7–C_{25}), NIST spectra dataset, Wiley libraries, and literature data.

2.3. Methodology for AgNPs Synthesis and Characterization

The adopted procedure from the previous literature report [31] with some minor modifications was used to optimize LTEO-AgNPs synthesis, and the reaction conditions were monitored using UV-Vis spectrometer (JASCO V-770, Tokyo, Japan). $AgNO_3$ solution was used as a blank for all UV-Vis measurements to adjust the baseline. For UV-Vis measurement LTEO-AgNPs solution was taken at end of the reaction. The colloidal solution of LTEO-AgNPs samples was adjusted to the same volume to obtain the uniform UV-Vis results using micropipette. 300 µL of the colloidal solution was taken and added to cuvette containing 2.4 mL double distilled water and mixed well before running UV-Vis

measurement. LTEO-AgNPs purification was performed by centrifuging the colloidal solution at 8000 rpm for 15 min and the obtained crystals were washed repeatedly three times with the minimum amount of double distilled water to remove impurities. Then, the purified pellets were dissolved in the optimum volume of double distilled water to minimize the aggregation effect of NPs and the colloidal solution was stored in brown bottle for the further analysis or applications. Optimization of reaction parameters for LTEO-AgNPs was based on a varying one factor at a time method [18]. Optimizing pH for the synthesis of LTEO-AgNPs was carried out by using the various pH of $AgNO_3$ solution at 3, 5, 7, 8, 9, 11, and 12. The adjustment of pH values was done using 0.1 M HCl or 0.1 M NaOH solutions. 4×10^{-4} M, 2×10^{-3} M, 6×10^{-3} M, 8×10^{-3} M, and 9×10^{-3} M $AgNO_3$ solution were used to determine the optimum $AgNO_3$ concentration conditions for the synthesis of LTEO-AgNPs. The effect of volumes of $AgNO_3$ solution was optimized using 70, 90, 110, and 130 mL of solution for the synthesis of LTEO-AgNPs. 15, 20, and 30 mL of LTEO solution (1 mL of LTEO in 170 mL of acetone) were used for the determination of optimum volume for the synthesis of LTEO-AgNPs. The sample of LTEO-AgNPs solution was taken for every reaction temperature at 45, 55, 60, 75, and 90 °C and the optimum reaction temperature was determined for the synthesis of LTEO-AgNPs. Reaction time was optimized for the synthesis of LTEO-AgNPs at 20, 30, and 40 min. Finally, the optimum reaction parameters were used for the synthesis of LTEO-AgNPs. In all reaction processes of LTEO-AgNPs synthesis, magnetic stirrer hot plate was used for the time and temperature controls and as a source of heat while UV-Vis spectroscopy was employed for the determination of SPR intensity peaks.

UV-Vis spectra were measured based on the procedure reported by [32] in the 300–700 nm range using a spectrophotometer (JASCO V-770, Tokyo, Japan) and $AgNO_3$ solution as a blank to adjust the baseline. The Fourier transform infrared (FT-IR) spectra of LTEO and LTEO-AgNPs were recorded using a FT-IR spectrophotometer (iS50 ABX, Thermo Scientific, Waltham, MA, USA) to determine the potential functional groups that were cause for the reduction of Ag^+ ions into Ag^0 in LTEO-AgNPs, stabilizing, and capping of AgNPs. Based on the earlier procedure [15], FT-IR spectra were run as follows: Few drops of LTEO and LTEO-AgNPs samples were applied with a resolution of 4 cm^{-1}, the spectral range of 400–4000 cm^{-1}, and number of scans of 32. For the determination of surface morphology and elemental composition of LTEO-AgNPs, scanning electron microscope-energy dispersive X-ray spectroscopy (SEM-EDX) analyses were performed using SEM-EDX (SSX-550 SEM-EDX, Shimadzu Co., Kyoto, Japan) with Sigma 300 operated at 20 kV based on the procedure reported by Saha and co-workers [32] with some minor modifications. LTEO-AgNPs crystal structure was determined by X-ray diffractometer (Philips PW1710; Philips Co., Amsterdam, The Netherlands) with a tube containing an X-ray with a copper target emitting Cu-Kα line with 1.54 A° wavelength and Bragg's angle limit of $30° \leq 2\theta \leq 80°$ based on the procedure provided in the previous study [33].

Particle size and zeta potential analyser (Zetasizer nano ZS; Malvern Instruments, Malvern, UK) was employed to determine the average size and surface potential of LTEO-AgNPs according to the procedure reported by the previous literature review [34]. The storage stability of LTEO-AgNPs was determined in the specific time intervals using the UV-Vis spectroscopic analysis based on the protocol reported previously by Gul et al. [35]. LTEO-AgNPs solution was stored deliberately at two different temperature conditions: 4 °C and room temperature. Then, the stability changes of sample was monitored by using UV-Vis spectroscopy for over 6 months.

2.4. Potential Applications of LTEO-AgNPs

For the investigation of potential activities of LTEO-AgNPs solution, antibacterial activity, seeds germination and seedlings growth test, colorimetric probes, and catalytic reduction activity were used as areas of application. The well diffusion method was applied for evaluating the antibacterial activities of different concentrations of LTEO-AgNPs solution as described by Vilas et al. [18] with some minor modifications. Three

Gram-positive pathogenic bacteria species such as *Staphylococcus aureus* (ATCC 25923), *Staphylococcus epidermidis* (ATCC 12228), and *Streptococcus agalactiae* (ATCC 12386) and three Gram-negative pathogenic bacteria species such as *Escherichia coli* (ATCC 25922), *Proteus mirabilis* (ATCC 35659), and *Pseudomonas aeruginosa* (ATCC 27853) were used for the antibacterial activity evaluation of LTEO-AgNPs solution. All bacteria species were provided by the Traditional and Modern Medicines Research Laboratory, Ethiopian Public Health Institute, Addis Ababa, Ethiopia. Ciprofloxacin (positive control) was obtained from Cadila Pharmaceuticals plc, Gelan, Oromia Regional State, Ethiopia. The overnight cultures of bacteria species were prepared in Luria-Bertani (LB) broth media. The prepared Muller-Hinton agar (MHA) solution (20 mL) was added to the sterilized Petri dish plates and then allowed for solidification. A number of 8 mm diameter circular wells were prepared, for ciprofloxacin, negative control (Tween-80) and LTEO-AgNPs solutions, in the MHA plate by using a sterile Cork borer. 120 µL of equal concentrations of controls and LTEO-AgNPs solutions were poured into the wells and allowed for incubation for 24 h at 37 °C. Zone of inhibition diameters (ZID) were recorded by using the millimeter scale. Percentage of relative zone of inhibition diameters (%RZID) of concentrations of LTEO-AgNPs solution was also calculated and used to compare these values with the control solutions.

Triticum aestivum (wheat) seeds germination and seedling growth test was conducted based on the procedure of Budhani and co-workers [36] with some minor modifications. The wheat seeds were sterilized with a 70% ethanol solution before the application. Next, the seeds were soaked in LTEO-AgNPs solution for 20 min (except for the control seeds) and finally, sown in a Petri dish with four pieces of filter paper and allow for germination. In each Petri dish, five healthy seeds were exposed to 0, 100, 500, 1000, and 2000 µL of LTEO-AgNPs solution (60 µg/mL) using double distilled water (DDH_2O) as a positive control. The experiments were conducted in three replicates. After 10 days of incubation, the percentage of seeds germination was calculated as %GS = $(n/N) \times 100\%$, where GS represents germination of seeds, n represents the total number of germinated seeds, and N represents the total number of seeds in germination test. The length of the root and shoot of seedlings were also measured on centimeter scale.

Selectivity and sensitivity determination of various metal ions tests were performed according to the previous report by Kalam and co-workers [37]. Selectivity tests of metal ions was studied by mixing 10 mL of solution, 2×10^{-3} M, of metal ions of Fe^{3+}, Ni^{2+}, Cu^{2+}, Zn^{2+}, Hg^{2+}, Cd^{2+}, K^{+}, Mg^{2+}, Al^{3+}, Cr^{6+}, Mn^{2+}, and Pb^{2+} with 10 mL of LTEO-AgNPs (60 µg/mL) solution in the transparent glass vials. Subsequently, the color change of the mixed solutions was visually examined, and the absorption spectra were monitored by UV-Vis spectroscopy after 30 min incubation period of time. The sensitivity of LTEO-AgNPs towards concentration of Hg^{2+} ions was also examined using various concentrations of Hg^{2+} ions solution in their decreasing order: 2×10^{-3}, 1.5×10^{-3}, 1.0×10^{-3}, 0.9×10^{-3}, 0.7×10^{-3}, 0.5×10^{-3} and 0.2×10^{-3} M solutions in the transparent glass vials. LTEO-AgNPs solution limit of detection (LOD) for the concentration of Hg^{2+} ions were evaluated by the color change visualization and controlling the UV-Vis absorption peaks of mixed solutions. Standards and samples were prepared under the same conditions and the experiments were carried out in three replicates. For selectivity and sensitivity tests, photographs of the appearance of solutions were taken with a digital camera.

The reduction of para nitrophenol (*p*-NP) to para-aminophenol (*p*-AP) was catalyzed using LTEO-AgNPs according to the procedure provided by Li and co-workers [38] to evaluate the reduction process using freshly prepared $NaBH_4$ solution as a mild reducing agent. To investigate the catalytic activity of LTEO-AgNPs, 2 mL of 2×10^{-3} M *p*-NP in 20 mL of the aqueous solution was added to 4 mL of 0.5 M $NaBH_4$ solution and stirring for 15 min and followed by the addition of 300 µL of LTEO-AgNPs solution (60 µg/mL) and stirred for 5 min more. Progress of the reaction had been traced with the decrease in UV-Vis absorbance peaks versus time for LTEO-AgNPs at 420 nm wavelength.

2.5. Statistical Analysis

All experimental activities were performed in three replicates. The data were subjected to one-way analysis of variance (ANOVA) using IBM SPSS statistics 26 software. Experimental values were expressed as mean ± standard deviation (SD). $p < 0.05$ were accepted as statistically significant.

3. Results and Discussion

3.1. Instrumental Analyses of LTEO

LTEO of a yellow color and pleasant odor was isolated from the powder of plant sample (dry weight). The total percentage yield of LTEO was 1.15%. The optical rotation (°α), refractive index (n_D), and specific gravity of the LTEO were obtained as +5.93° (at 25.5 °C), 1.49118 (at 20 °C) and 0.1179 (at 20 °C), respectively. LTEO was highly soluble in 90% ethanol. Some results were reported by earlier study [28] on the aerial part of *L. tomentosa* but with lower percentage yield of EO (0.50%). The analysis of GC-MS of LTEO depicted a total of 38 chemical compounds for constituents greater than 0.11% area percentage which account for a total of 87.97%. The identified chemical compounds represent monoterpenes (51.58%), sesquiterpenes (28.10%) and some other hydrocarbons (8.29%). The corresponding Kovat's indices from literature review and chemical structures of some components with 11.73% of total area percentage could not be obtained from the NIST spectra dataset while their experimental (calculated) Kovat's indices were determined. The first 11 identified chemical constituents of LTEO such as eucarvone (25.74%), 2,5-dimethoxy-*p*-cymene (9.39%), (-)-germacrene D (8.49%), chrysanthenone (6.81%), 2,5-dimethylphenol (5.23%), E-ocimenone (3.45%), γ-curcumin (3.33%), 2,6-dimethylphenol (2.92%), β-cubenene (2.57%), 4,6,6-trimethylbicyclo[3.1.1]hept-3-en-2-one (2.08%) and humulene (2.00%) which represent about 72.01% of the total composition are presented in Figure 1. The dominant chemical constituents of LTEO contain the oxygenated, olefinic, aromatic, and cyclic functional groups. In some previous studies, chrysanthenone (57.5%) and 2,5-dimethoxy-*p*-cymene (64.76%) were reported by Asfaw et al. [28] and Getahun et al. [30], respectively as major components of essential oil of aerial part of *L. tomentosa*. However, in this research work, eucarvone is reported for the first time as major components from this plant species.

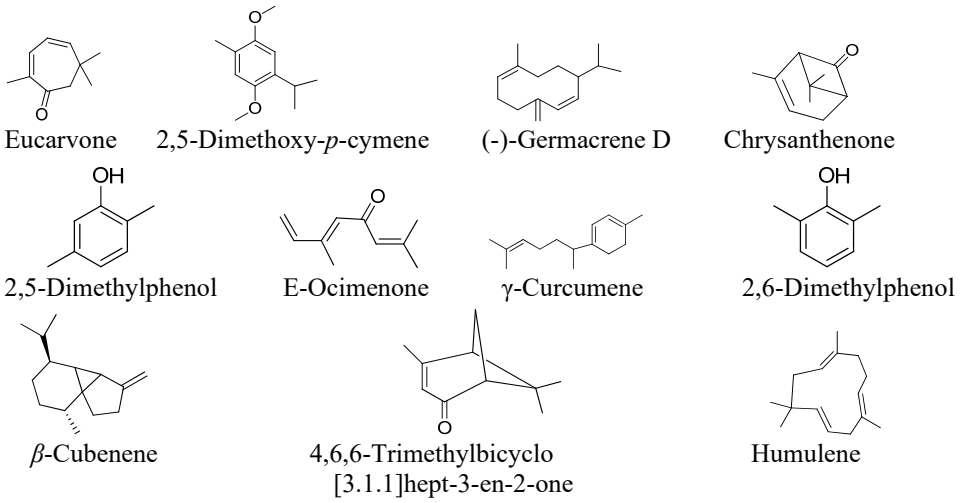

Figure 1. Structures of the first 11 main constituents of LTEO (for peak area ≥ 2%).

As shown in Figure 2, FT-IR spectra of LTEO showed the presence of sp^3C-H symmetric bond stretching (2947 cm^{-1}), carbonyl group (1774 cm^{-1}), aromatic C=C symmetric bond stretching (1446 cm^{-1}), sp^2C-O symmetric bond stretching (1208 cm^{-1}) and aromatic C-H in plane bond bending (1020 cm^{-1}). The demonstrated FT-IR spectra of LTEO were more probably for major functional groups of oxygenated compounds and aromatic compounds. Moreover, the functional groups of chemical constituents of LTEO are supported by the

existing literature review [33,39] and the structures of chemical compounds identified by GC/MS analysis in this study.

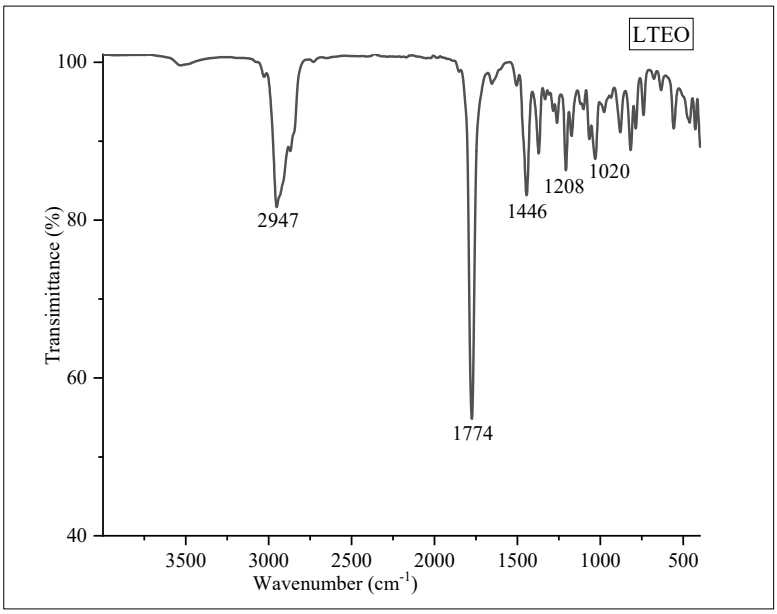

Figure 2. FT-IR spectrum of essential oil of aerial part of *L. tomentosa* (LTEO).

3.2. Optimization, Synthesis, and Characterization of LTEO-AgNPs

3.2.1. Optimization Process

Optimization of reaction parameters plays a crucial role in determining a cost-effective, simple, and time-efficient method to improve the homogeneity of NPs [40]. The effects of reaction parameters on LTEO-AgNPs synthesis were evaluated using the one factor-at-a-time method [41,42]. The observed maximum UV-Vis absorbance peak for the LTEO-AgNPs solution was considered optimum parameter. Different pH values at 3, 5, 7, 8, 9, 11, and 12 were used to determine the optimum pH of $AgNO_3$ solution for the synthesis of LTEO-AgNPs. There was no formation of LTEO-AgNPs in the acidic condition (at pH 3 and 5). This result is consistent with the result reported by the previous literature article [9]. In acidic conditions, the produced LTEO-AgNPs were not stable enough and as a result NPs led to agglomeration. At neutral and basic conditions (at pH 7, 8, 9, 11, and 12), intense peaks were observed in the UV-Vis region of AgNPs. These results effectively confirmed the formation of LTEO-AgNPs in neutral and basic conditions. However, the optimum reaction pH was found at 11 (Figure 3a). Various concentrations of $AgNO_3$ solution such as 4×10^{-4} M, 2×10^{-3} M, 4×10^{-3} M, 6×10^{-3} M, 8×10^{-3} M, and 9×10^{-3} M were used to study their effects on the synthesis of LTEO-AgNPs. 2×10^{-3} M $AgNO_3$ solution was obtained as optimum concentration with the maximum absorbance peak intensity in the UV-Vis region of AgNPs (Figure 3b). The absence of UV-Vis peaks at higher concentrations of $AgNO_3$ solution (8×10^{-3} M and 9×10^{-3} M) may be due to the excess concentration accelerating the aggregation of AgNPs [43].

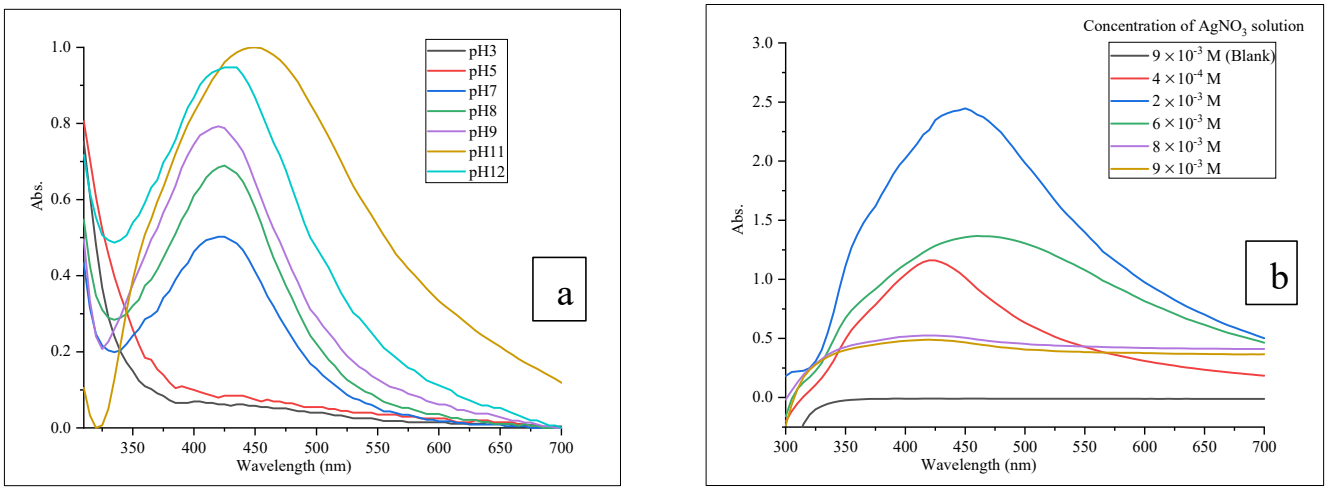

Figure 3. UV-Vis graph of (**a**) pH and (**b**) concentrations of $AgNO_3$ solution optimization.

The reactants used for AgNPs synthesis were $AgNO_3$ and LTEO solutions. $AgNO_3$ solution was used as Ag precursors while LTEO solution applied as bioreductant in AgNPs synthesis. The volume of $AgNO_3$ solution: 70, 90, 110, and 130 mL were employed to determine the optimum volume of $AgNO_3$ solution required for the high yield of LTEO-AgNPs formation. 70 mL of $AgNO_3$ solution produced LTEO-AgNPs with maximum UV-Vis absorbance (Figure 4a). To examine the effect of various volumes of bioreductant solution on the synthesis of AgNPs, 15, 20, and 30 mL of LTEO solution were used. The optimum volume of bioreductant solution was obtained as 20 mL (Figure 4b) for LTEO-AgNPs formation. The decreasing effect of UV-Vis absorbance peak at higher volume of LTEO solution (30 mL) was due to the inaccessibility of functional groups in LTEO for Ag^+ ions because of the competition between bioreductant components and Ag^+ ions [44].

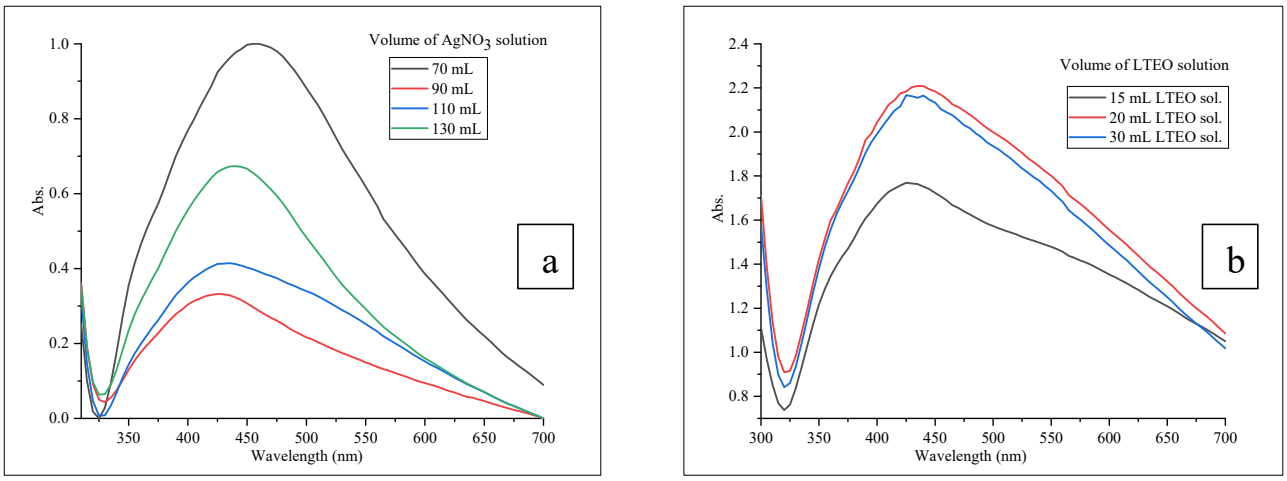

Figure 4. UV-Vis graph of volume of (**a**) $AgNO_3$ and (**b**) LTEO solutions optimization.

Temperature and time were also the important reaction parameters to be optimized for the synthesis of AgNPs. The reaction temperature showed different effects on the nucleation and growth of AgNPs [45]. In LTEO-AgNPs synthesis, the reaction temperatures set at 45, 55, 60, 75, and 90 °C (Figure 5a) using the magnetic stirrer digital hot plate. The decreasing of UV-Vis absorbance of LTEO-AgNPs at 90 °C may be attributed to the slow nucleation of AgNPs due to the formation of their larger size [46]. Therefore, the optimum reaction temperature for the synthesis of LTEO-AgNPs was obtained at 75 °C as the maximum UV-Vis absorbance.

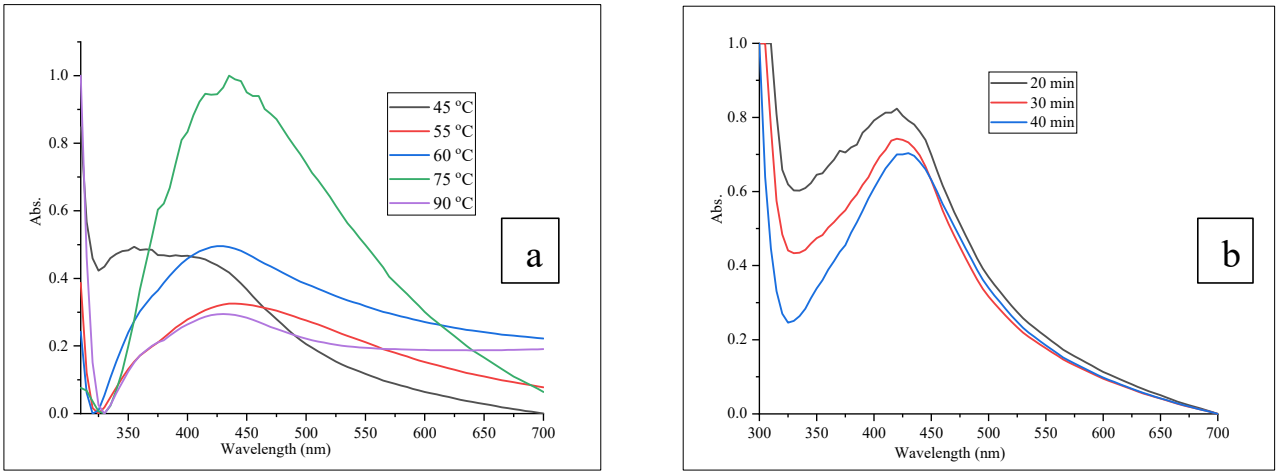

Figure 5. UV-Vis graph of (**a**) temperature and (**b**) time of reaction optimization.

Time of reaction optimization was performed at 20, 30, and 40 min. The effective optimum reaction time was obtained at 20 min (Figure 5b). The lower UV-Vis absorbance peaks at higher reaction times (at 30 and 40 min) were due to the aggregation of NPs over nucleation as the reaction time increases [47].

3.2.2. Synthesis of LTEO-AgNPs

Finally, LTEO-AgNPs were synthesized using the optimum reaction parameters all at once together. 70 mL of 2×10^{-3} M $AgNO_3$ solution was adjusted to pH 11 and boiled to 75 °C while stirring on the magnetic stirrer digital hot plat. 20 mL of LTEO solution was added slowly in drop-wise to the boiling $AgNO_3$ solution. After 20 min, the characteristic brown color of AgNPs colloidal solution was observed and the formation was confirmed by using UV-Vis spectroscopy. The proposed mechanism of LTEO-AgNPs is given in Figure 6.

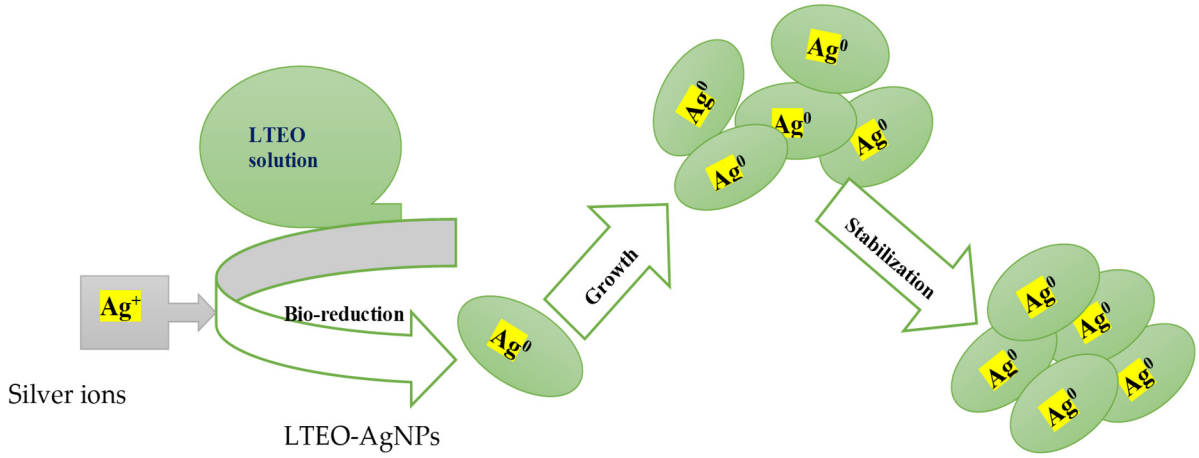

Figure 6. The proposed mechanism for the synthesis of LTEO-AgNPs.

3.2.3. Characterization of LTEO-AgNPs

UV-Vis spectra of LTEO-AgNPs colloidal solution were assessed by measuring their absorption spectrum using UV-Vis spectroscopy over 300–700 nm range, as shown in Figure 7a. A characteristic absorption peak was observed at 420 nm due to the surface plasmon resonance (SPR) of AgNPs. Therefore, formation of LTEO-AgNPs was confirmed by brown color visualization and absorption of SPR peak between 400–450 nm. The observed peak was in the normal UV-Vis absorption range for AgNPs. The broadening of LTEO-AgNPs UV-Vis spectrum may be because of the aggregation effect of NPs [45].

The brown color of the AgNPs colloidal solution was due to the excitation and collective oscillation of free electrons on the surface of AgNPs, which interact with light waves [48,49]. The combined FT-IR spectra of LTEO and LTEO-AgNPs are depicted in Figure 7b. FT-IR spectrum of LTEO-AgNPs showed dominant peaks at 3272 cm^{-1} and 1634 cm^{-1} in the functional group region. These peaks indicated the presence of -O-H and C=O functional groups on the surface of synthesized AgNPs [15,50]. The functional groups mainly present on the surface of LTEO-AgNPs were –O-H and C=O. This effect indicated the functional groups of chemical constituents of LTEO were involved in the reducing, capping, and stabilizing action of LTEO-AgNPs formation.

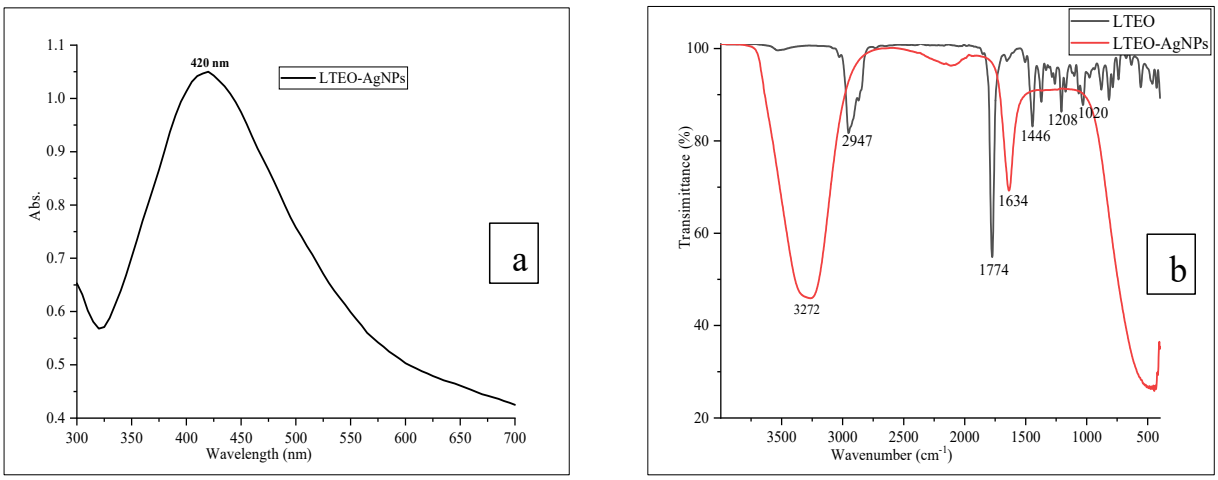

Figure 7. UV-Vis graph of (**a**) optimized LTEO-AgNPs and (**b**) the combined FT-IR spectra of LTEO and LTEO-AgNPs.

ImageJ software was used for the analysis of NPs size measurements by considering different sizes of LTEO-AgNPs. SEM images of LTEO-AgNPs demonstrated that the shapes of NPs are predominantly spherical, with average size of 89.59 ± 5.14 nm, Figure 8a. EDX showed the presence of Ag element at about 3.0 keV in the synthesized AgNPs [51]. In Figure 8b, the two intense peaks in EDX spectrum clearly confirmed the presence of Ag elements and the formation of AgNPs.

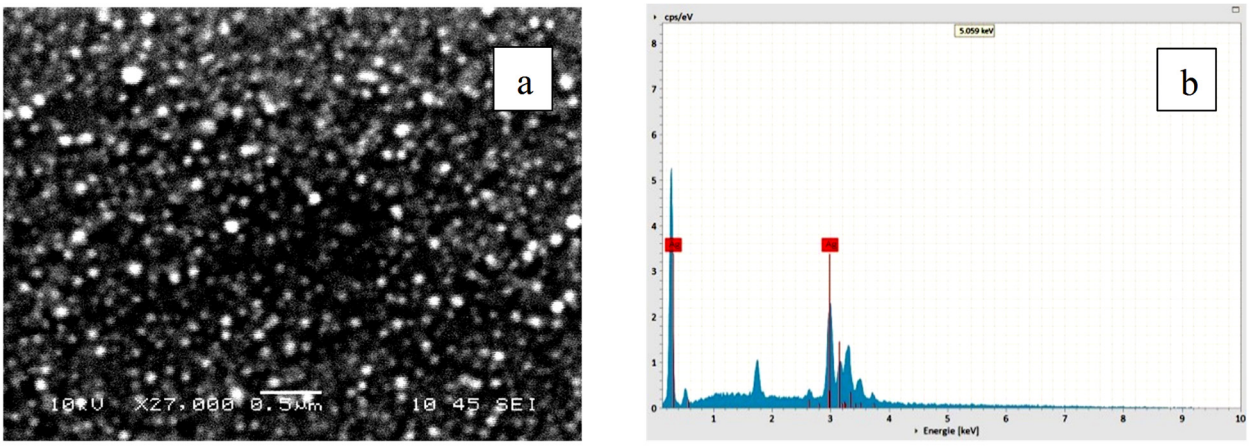

Figure 8. (**a**) SEM and (**b**) EDX images of LTEO-AgNPs.

XRD analysis is used for the determination of unknown crystalline nanomaterials [52]. Three dominant XRD peaks were observed at 38°, 44° and 67° in the 2θ range to represent the characteristic peaks of AgNPs formation (Figure 9). The peaks can be assigned to (111), (200) and (220), respectively which confirmed the face-centered cubic structures of

silver. The XRD analysis is in good agreement with the green AgNPs synthesized using *C. roxburghii* aqueous extract [2]. XRD peaks of AgNPs prepared using the rhizome extract of *C. orchioides* in the earlier study and reported with the Joint Committee on Powder Diffraction Standards (JCPDS) card No. 04-0783 [32] further supported the XRD peaks pattern of LTEO-AgNPs.

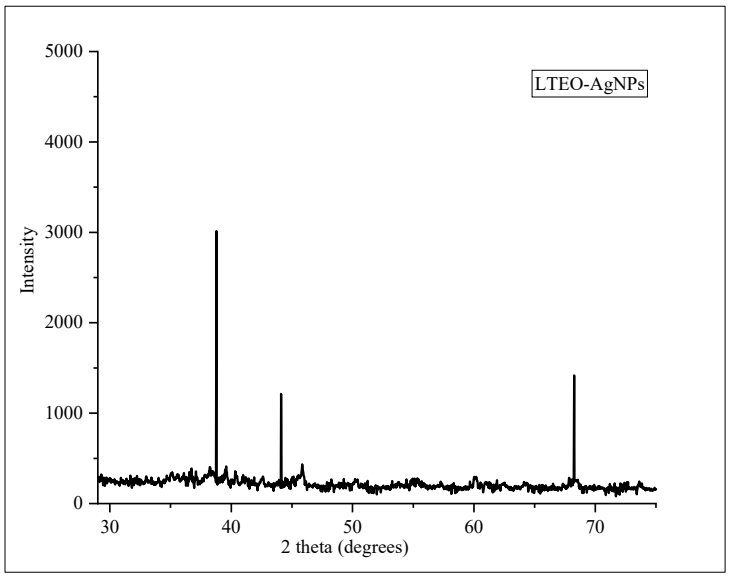

Figure 9. The XRD peaks of LTEO-AgNPs.

The average size and surface potential of synthesized AgNPs were determined by using the nanosizer analysis technique. The measurement of NPs size distribution was shown in Figure 10a and the average size and polydispersity index (PDI) of LTEO-AgNPs were obtained as 94.98 nm (diameter) and 0.241, respectively. The small value of PDI is reported to inform the homogeneity of the size of AgNPs [53]. Zeta potential of NPs determines the electrostatic attraction or repulsion nature on their surface [54]. Therefore, the value of zeta potential was used for a rough indication of the stability of synthesized AgNPs. Values greater than ±30 mV indicate the stability of synthesized nanomaterials [55]. Therefore, the determined magnitude of zeta potential, −49.5 mV (Figure 10b), with an overall negative charge on the surface of synthesized AgNPs, roughly predicted the stability of LTEO-AgNPs, which is supported by the existing literature reports [36].

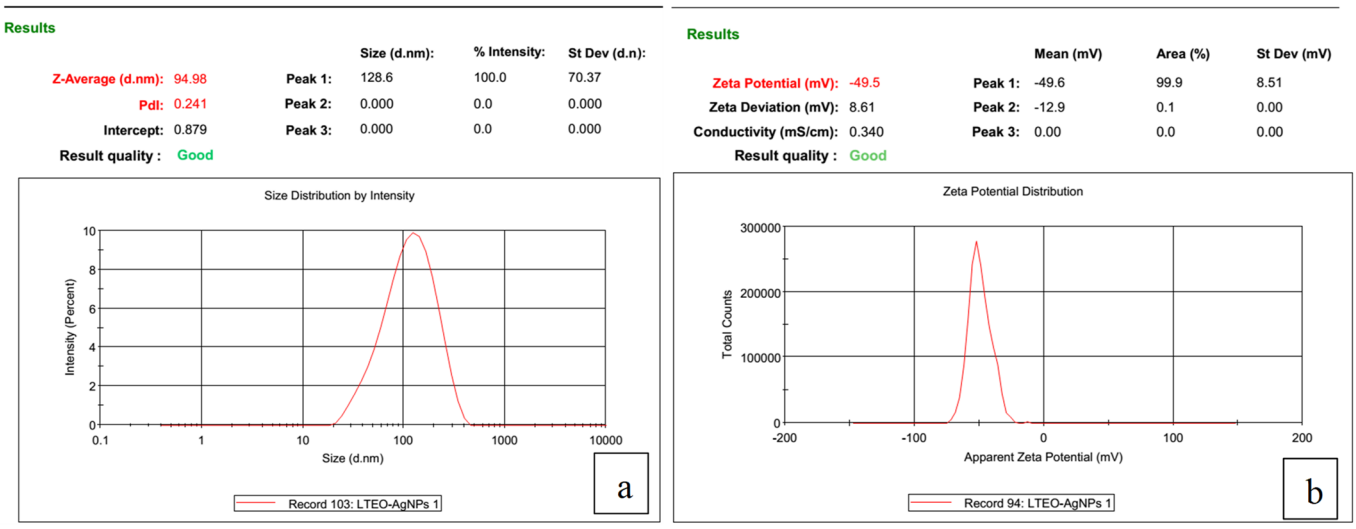

Figure 10. (**a**) Zeta size and (**b**) zeta potential of LTEO-AgNPs.

Stability is one of the parameters that ensures the life span of AgNPs can be used effectively in different application areas [33,37,56]. The physicochemical stability of LTEO-AgNPs was studied over 6 months using UV-Vis spectra analysis. LTEO-AgNPs samples were stored at 4 °C and room temperature, separately. They revealed wide variation in the SPR peaks after a month on the stability of LTEO-AgNPs (Figure 11a,b).

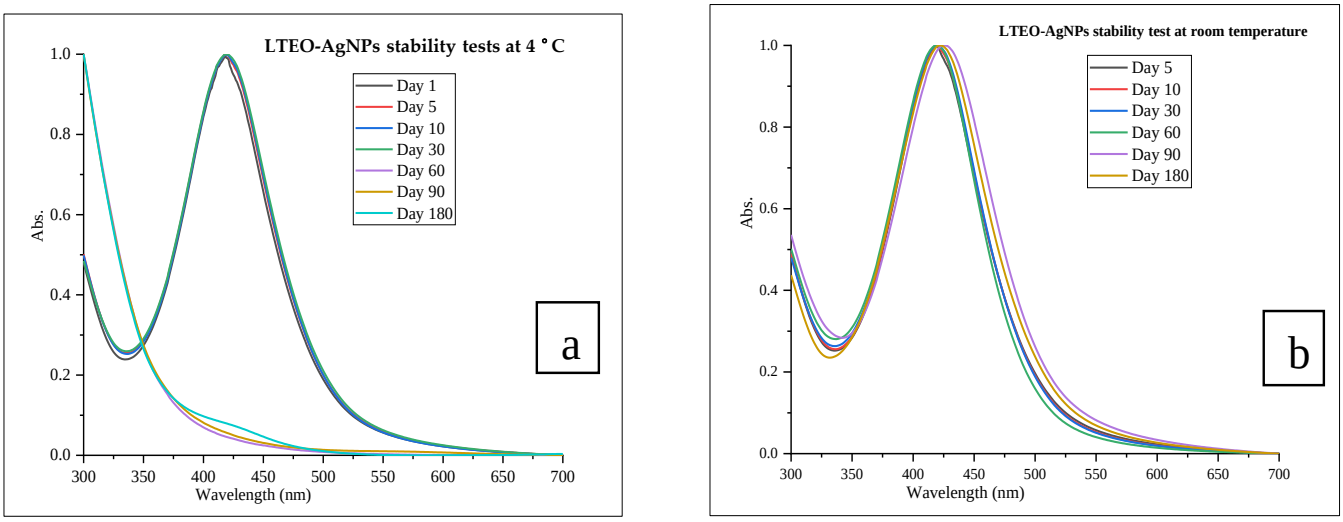

Figure 11. UV-Vis graphs for stability tests of LTEO-AgNPs over 90 days at (**a**) 4 °C and (**b**) room temperature.

In this study, the synthesized AgNPs showed stronger stability at room temperature for over 6 months. These results demonstrated that better stability of LTEO-AgNPs against aggregation or dissolution was observed at room temperature than at 4 °C. The aggregation or dissolution effect of LTEO-AgNPs at 4 °C (in the refrigerator) might be resulted because of the oxidation of Ag° into Ag+ ions or recrystallization of colloidal solution of AgNPs [12].

3.3. Applications of LTEO-AgNPs

3.3.1. Antibacterial Activity

Antibacterial activities of LTEO-AgNPs solution was evaluated for pathogenic bacteria species using Gram-positive strains: *S. epidermidis*, *S. aureus*, and *S. agalactiae* and Gram-negative strains: *P. mirabilis*, *E. coli*, and *P. aeruginosa*. The concentrations of LTEO-AgNPs solution were prepared from full strength or 100% LTEO-AgNPs solution (60 µg/mL) to 6.25% LTEO-AgNPs solution using the dilution series method. Besides, LTEO solution (60 µg/mL) was adjusted to 30% LTEO solution and used as the reference control in the antibacterial activity assay. LTEO-AgNPs solutions demonstrated the inhibition of bacteria growth except for 12.5% LTEO-AgNPs solution against *P. aeruginosa* and 12.5% and 6.25% LTEO-AgNPs solution against *P. mirabilis*. The 30% LTEO solution, a control, demonstrated higher activity than all concentrations of its AgNPs solution against the test bacteria species growth. For example, the maximum and minimum ZID values of 30% LTEO solution were obtained as 24.33 ± 0.58 and 13.33 ± 0.58 mm against *S. aureus* and *S. agalactia*, respectively. However, at full strength of LTEO-AgNPs solution (100% LTEO-AgNPs solution), ZID values were recorded in the range of 21.00 ± 1.00 to 11.00 ± 1.00 mm while at the minimum concentration of LTEO-AgNPs solution (6.25% LTEO-AgNPs solution), ZID values were determined in the range of 11.00 ± 1.00 to 0.00 mm for all tests bacteria species. Therefore, all tests' bacteria species showed stronger resistance to the concentrations of LTEO-AgNPs solution than 30% LTEO solution (a reference control) and ciprofloxacin (a positive control). The obtained results are in contrast to the previous research findings on the antibacterial activity of plant extracts and their AgNPs. In the earlier literature report, plant extracts were obtained weaker antibacterial activity than their AgNPs [18,57].

The zone of inhibition diameters (ZID, mm) of full strength to 6.25% LTEO-AgNPs solution against all bacterial strains were summarized and presented in Table 1. The percentage of the relative zone of inhibition diameter (%RZID) for the antibacterial activity of LTEO-AgNPs solution was calculated and presented in Table 2. The ZID or %RZID values were compared with controls such as 5 µg/mL ciprofloxacin, 30% LTEO and 5% Tween-80 (in sterilized distilled water) solutions. The results of ZID or %RZID of the synthesized AgNPs solution are the mean ± SD of three replicates and statistically significant at $p < 0.05$.

Table 1. Antibacterial activity of various concentrations of LTEO-AgNPs solution against the test pathogenic bacteria species using the agar well diffusion method.

Test Microorganism	Zone of Inhibition Diameter (ZID) * in mm						
	Cipro. (5 µg/mL)	LTEO Sol. (30%)	LTEO-AgNPs (Full Strength)	50% LTEO-AgNPs	25% LTEO-AgNPs	12.5% LTEO-AgNPs	6.25% LTEO-AgNPs
S. aureus	26.00 ± 0.00	24.33 ± 0.58	21. 00 ± 1.00	20.67 ± 0.58	12.67 ± 0.58	9.00 ± 0.00	9.00 ± 0.00
S. epidermidis	34.33 ± 1.15	23.33 ± 0.58	16.67 ± 0.58	14.33 ± 0.58	12.00 ± 0.00	11.00 ± 0.00	9.67 ± 0.58
S. agalactiae	21.33 ± 1.53	13.33 ± 0.58	11.67 ± 0.58	10.00 ± 0.00	9.00 ± 0.00	8.67 ± 0.58	8.33 ± 0.58
E. coli	33.33 ± 0.58	18.33 ± 0.58	20.33 ± 0.58	19.00 ± 1.00	15.33 ± 0.58	12.67 ± 0.58	11.00 ± 1.00
P. mirabilis	39.33 ± 0.58	16.33 ± 1.15	11.00 ± 1.00	11.33 ± 0.58	9.00 ± 0.00	8.00 ± 0.00	8.00 ± 0.00
P. aeruginosa	31.33 ± 0.58	14.67 ± 0.58	13.67 ± 0.58	13.33 ± 0.58	11.67 ± 0.58	9.33 ± 0.58	8.00 ± 0.00

* ZID results were expressed as mean ± SD of three replicates; LTEO—*L. tomentosa* essential oil, Cipro.—Ciprofloxacin (Positive control), Tween-80 (Negative control), ZID values including well diameter, 8 mm, $p < 0.05$ is considered as statistically significant value.

Table 2. Percentage of the relative zone of inhibition diameter of different concentrations of LTEO-AgNPs solution against test bacteria species.

Test Microorganism	%RZID *						
	Cipro.	LTEO Sol. (30%)	LTEO-AgNPs (Full Strength)	50% LTEO-AgNPs	25% LTEO-AgNPs	12.5% LTEO-AgNPs	6.25% LTEO-AgNPs
S. aureus	100.00 ± 0	90.75 ± 3.22	72.22 ± 5.56	70.37 ± 3.20	25.93 ± 3.21	5.56 ± 0	5.56 ± 0
S. epidermidis	100.00 ± 0	58.27 ± 2.38	32.99 ± 3.20	24.15 ± 3.34	15.21 ± 0.68	11.41 ± 0.51	6.37 ± 2.33
S. agalactiae	100.00 ± 0	40.60 ± 8.54	28.03 ± 7.07	15.13 ± 1.69	7.56 ± 0.84	5.34 ± 4.64	2.22 ± 3.85
E. coli	100.00 ± 0	40.77 ± 1.33	48.72 ± 2.99	43.44 ± 4.12	28.97 ± 2.69	18.41 ± 2.12	11.80 ± 3.70
P. mirabilis	100.00 ± 0	26.57 ± 3.50	9.61 ± 3.33	10.62 ± 1.63	3.20 ± 0.08	0.00	0.00
P. aeruginosa	100.00 ± 0	28.63 ± 3.14	23.94 ± 1.91	22.89 ± 2.81	15.70 ± 2.33	5.74 ± 2.57	0.00

* %RZID results were expressed as mean +SD of three replicates; LTEO—*L. tomentosa* essential oil, Cipro.—Ciprofloxacin (Positive control), Tween-80 (Negative control), $p < 0.05$ is considered as statistically significant values.

Based on the results presented in Tables 1 and 2, most of the concentrations of synthesized AgNPs solution exhibited significant ($p < 0.05$) inhibition activities against bacterial strains. Comparing to ciprofloxacin (the wide spectrum antibiotic drug), full strength of LTEO-AgNPs solution exhibited about 72.22 ± 5.56%, 48.72 ± 2.99%, and 32.99 ± 3.20% inhibition of *S. aureus*, *E. coli*, *S. epidermidis* growth, respectively. *S. aureus*, *E. coli*, and *S. epidermidis* were also strongly susceptible to all concentrations of the synthesized AgNPs solution while *P. mirabilis* and *P. aeruginosa* exhibited higher resistance to the lower concentrations of LTEO-AgNPs solution. The significant differences ($p < 0.05$) of antibacterial activity of various concentrations of LTEO-AgNPs solution against pathogenic bacteria species were further supported by the multiple comparisons between ZID and %RZID values. Even though the exact mechanism of LTEO-AgNPs against pathogenic bacteria species were not determined, their actions can be hypothesized based on the previous studies. LTEO-AgNPs enter the cell membrane of bacteria and release Ag^+ ions when it contacts with moisture. Then, Ag^+ ions can disrupt the activity of cell membrane of bacteria and lead to their cell death [7,18].

3.3.2. Seeds Germination and Seedlings Growth

The impact of various concentrations of LTEO-AgNPs solution on *T. aestivum* seeds germination and seedlings growth was evaluated every 24 h for each treatment. After 10 days, the recorded data on the percentage of seeds germination and the length of root and shoot of seedlings were analyzed and provided in Table 3. The germination rates of seeds of *T. aestivum* were ranged from 93.33% to 100% and there was no observable statistically significant difference between the control and concentrations of LTEO-AgNPs solution. From the test solutions, only 2000 of LTEO-AgNPs solution (100 µg/mL) had statistically significant ($p < 0.05$) effect on the elongation of root and shoot of *T. aestivum* seedlings. The LTEO-AgNPs solution displayed adverse effects on the growth of *T. aestivum* seedlings at lower volumes (100, 500, and 1000 µL) compared to the control treatment, which was supported by post hoc multiple comparisons between values. Still at these volumes, LTEO-AgNPs solution showed stronger enhancement in the roots' elongation (11.05 ± 7.44 to 11.91 ± 3.13) than shoots part (8.23 ± 5.60 to 9.50 ± 3.55) of seedlings. However, at 2000 µL LTEO-AgNPs solution, it enhanced the germination and seedlings growth of seeds of *T. aestivum* as compared to the positive control. Therefore, in this study, the increasing of volume of LTEO-AgNPs solution demonstrated the increasing of elongation effect in the treatment of seedlings of *T. aestivum*. In earlier study, such effects were reported to be depending on the types of NPs and plant extract's concentration [58]. Some recent studies also demonstrated green AgNPs exhibited both positive and negative effects on the length of root and shoot and germination rate of seedlings [36,55].

Table 3. LTEO-AgNPs effects on seeds germination and seedling growth of *T. aestivum*.

Treatment	Seeds Germination (%)	Seedling Elongation (in cm) *	
		Root	Shoot
PD0: Control(DDH_2O)	100.00 ± 0.00	15.47 ± 5.53	10.22 ± 4.20
PD100: LTEO-AgNPs (100 µL)	100.00 ± 0.00	11.05 ± 7.44	8.23 ± 5.60
PD500: LTEO-AgNPs (500 µL)	93.33 ± 0.00	11.63 ± 7.11	9.47 ± 5.55
PD1000: LTEO-AgNPs (1000 µL)	100.00 ± 0.00	11.91 ± 3.13	9.50 ± 3.55
PD2000: LTEO-AgNPs (2000 µL)	100.00 ± 0.00	17.03 ± 7.02	10.23 ± 4.89

* Calculated values were statistically significant difference at $p < 0.05$.

3.3.3. Colorimetric Detection of Metal Ions

LTEO-AgNPs solution and different metal ions were mixed in transparent glass vials and let stand for 30 min at room temperature. The results displayed selective decolorization which visualized through the naked eye only for Hg^{2+} ions, and their SPR band intensity was monitored using UV-Vis spectroscopy (Figure 12a,b). The absorption of UV-Vis spectra of LTEO-AgNPs solution at 420 nm disappeared completely on its mixing with Hg^{2+} ion solution.

Even though there was weakly fading of brown color of LTEO-AgNPs solution on its addition with Fe^{3+}, Cu^{2+}, Al^{3+}, and Cr^{6+}ions solution, the UV-Vis absorption spectra analysis demonstrated the blue shift and peak narrowing for Cr^{6+} ions and redshift and peak broadening for Al^{3+}, Fe^{3+}, and Cu^{2+} ions. LTEO-AgNPs solution did not show detectable effect on the Ni^{2+}, Zn^{2+}, Cd^{2+}, K^{+}, Mg^{2+}, Mn^{2+}, and Pb^{2+} ions in the sample solution. The obtained result was in consistent with the colorimetric result reported by [37,43] regarding Ni^{2+}, Zn^{2+}, K^{+}, Mg^{2+}, and Hg^{2+} ions. The evaluation of selectivity detection of LTEO-AgNPs towards various metal ions resulted the rapid color change and strongest selective only towards Hg^{2+} ions over the other metal ions. The fast color change depicted that LTEO-AgNPs solution serve as promising probe for the qualitative analysis of Hg^{2+} ions in the real samples. UV-Vis spectra analysis showed that LTEO-AgNPs can be utilized for the determination of metal ions such as Cr^{6+}, Al^{3+}, Fe^{3+}, and Cu^{2+} ions in some environmental samples. The electrochemical series approach is used to explain the colorimetric detection mechanism of Hg^{2+} ions due to metals with higher electrochemical reduction potential showing a better tendency as oxidizing agents [59,60].

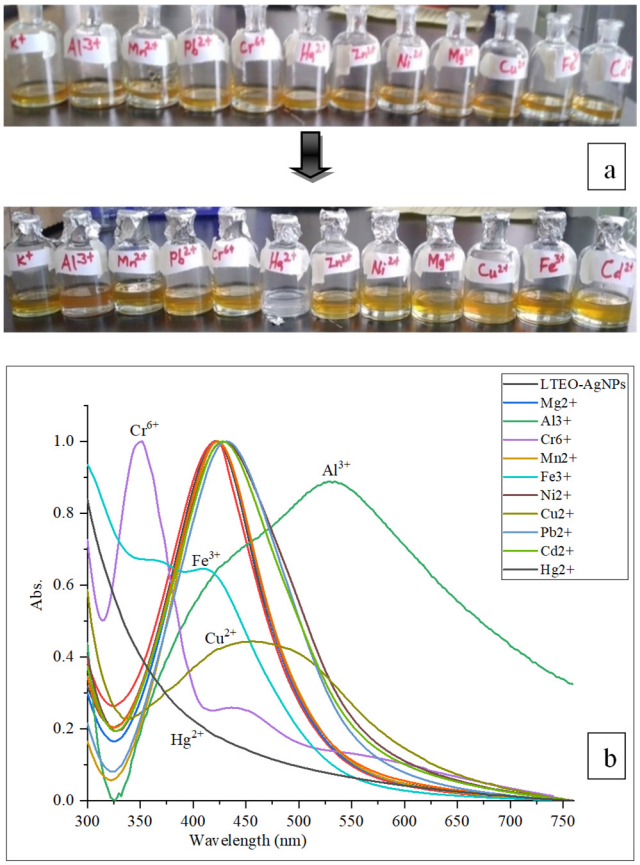

Figure 12. (**a**) Camera image of LTEO-AgNPs-metal ions mixtures (arrow indicates before and after decolorizing) and (**b**) UV-Vis absorbance spectra of LTEO-AgNPs and results of the mixture.

The disappearance of SPR peak of LTEO-AgNPs solution on mixing with Hg^{2+} ions was due to the elimination of stabilizing agents from the AgNPs and capping Hg^{2+} ions, i.e., aggregation of AgNPs or oxidation of Ag^0 to Ag^+ ions by Hg^{2+} ions, i.e., dissolution of AgNPs [43]. Further study was conducted to determine how low the concentration of Hg^{2+} ions can be detected by LTEO-AgNPs solution. Figure 13a,b showed the sensitivity tests of LTEO-AgNPs solution towards 2×10^{-3} M, 1.5×10^{-3} M, 1×10^{-3} M, 0.9×10^{-3} M, 0.7×10^{-3} M, 0.5×10^{-3} M, and 0.2×10^{-3} M Hg^{2+} ions. LTEO-AgNPs could detect concentration of Hg^{2+} ions up to 0.5×10^{-3} M. The detected minimum concentration of Hg^{2+} ions with LTEO-AgNPs solution (60 µg/mL) was not strong when compared to the previous research results reported for the other plants extracts mediated AgNPs.

3.3.4. Catalytic Reduction Activity

The schematic reaction for converting *p*-NP to *p*-AP using $NaBH_4$ with LTEO-AgNPs as a catalyst and UV-Vis monitoring were given in Figure 14a,b. The catalytic effect of LTEO-AgNPs was studied by using the reduction of *p*-NP to *p*-AP with excess $NaBH_4$ at room temperature. Reaction progress was controlled using UV-Vis spectroscopy. The characteristic peak absorption was recorded at 400 nm due to the formation of *p*-NPi, and the peak remained unchanged for a longer period of time. Then, after adding LTEO-AgNPs to the mixture solution, UV-Vis spectra analysis showed that the original peak intensity was declining as the time of reaction was increasing. For instance, the UV-Vis intensities of the mixture exhibited different intensities at the beginning, 20, and 40 min of reaction times (Figure 14b). This effect was observed due to the catalytic reduction of *p*-NPi to *p*-AP as a result of conversion of $-NO_2$ to $-NH_2$ in the presence of LTEO-AgNPs. The formation of *p*-AP was confirmed by the decreasing of the UV-Vis signal intensity at 400 nm and the appearance of a new UV-Vis peak at 297 nm. Several previous studies on the catalytic

reduction activity of nitrophenol derivatives to aminophenol compounds using biogenic AgNPs supported the result which reported in this study [38,51,61].

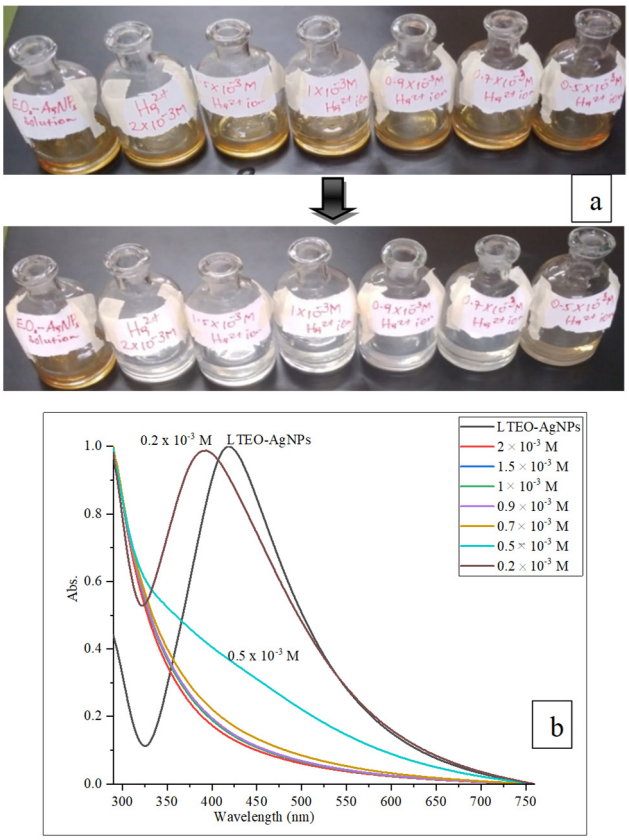

Figure 13. (**a**) Camera image of LTEO-AgNPs/Hg^{2+} ions mixture (arrow indicates before and after decolorizing) and (**b**) UV-Vis absorbance spectra of sensitivity test of LTEO-AgNPs towards different concentrations of Hg^{2+} ions.

Organic pollutants including nitrophenols are extensively used in laboratories and industrial processes as they are precursors for the preparations of different drugs, pesticides, and synthetic dyes [62,63]. Aminophenol compounds are important intermediates for the synthesis of paracetamol, phenacetin, sulphur dyes, rubber antioxidants, corrosion inhibitors and precursors in antipyretic and analgesic drugs [1,45]. Para aminophenol (*p*-AP) is the reduced product of para nitrophenol (*p*-NP) using efficient catalysts. The Maximum peak of *p*-NP at 400 nm immediately disappeared when it was reduced to *p*-AP [64]. Mild reducing agent $NaBH_4$ alone cannot reduce functional groups such as nitro (-NO_2) groups due to the presence of a kinetic barrier and the potential difference between donor, borohydride (BH_4^-) and acceptor, *p*-nitrophenolate ion (*p*-NPi). To overcome this kinetic barrier, metallic NPs such as AgNPs promote the reduction reaction by increasing the chance of electron transfer from donor to acceptor groups through adsorption of reactants on the surface of AgNPs to diminish the activation energy barriers. As a result of the adsorption of *p*-NPi and BH_4^- ions on the surface of AgNPs, catalytic reduction was facilitated by transfer of electron from BH_4^- ions to *p*-NPi to produce *p*-AP [38,42].

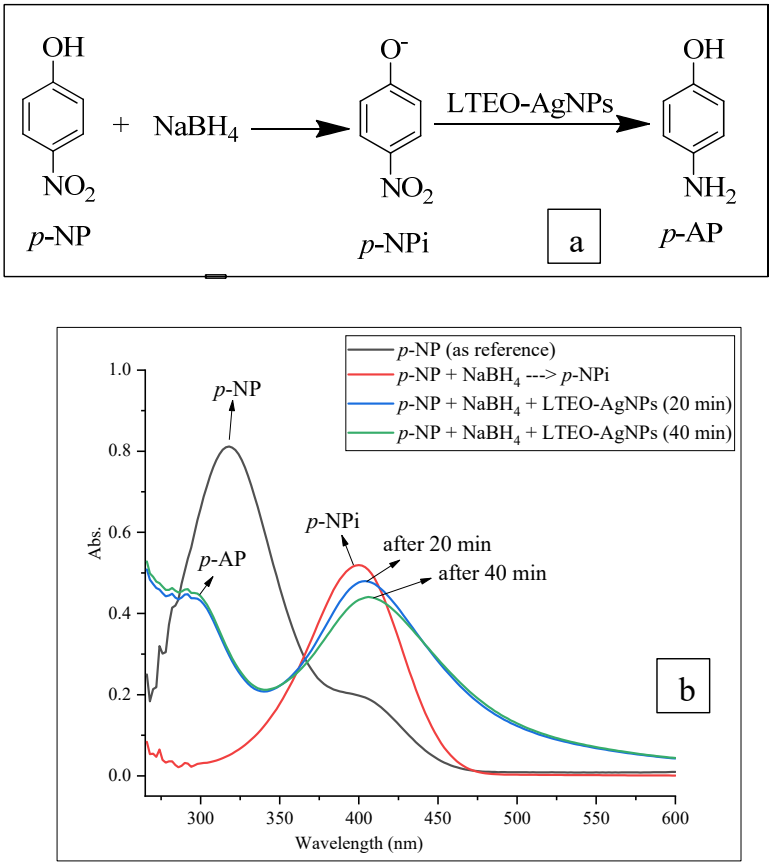

Figure 14. (**a**) Schematic representation for the catalytic reduction of *p*-NP to *p*-AP and (**b**) UV-Vis absorbance of *p*-NP, *p*-NPi and *p*-AP.

4. Conclusions

In this study, AgNPs were synthesized successfully using the essential oil was isolated from the aerial part of *L. tomentosa* by hydrodistillation method. GC/MS analysis exhibited monoterpenes and sesquiterpenes are the dominant classes and eucarvone was identified as the major chemical constituent of LTEO. The optimized reaction parameters: pH, the concentration of $AgNO_3$ solution, the volume of reactants, temperature, and time were used for LTEO-AgNPs preparation. FT-IR spectroscopy was also used to determine the major functional groups of chemical components of LTEO which may be important for the reduction of Ag^+ ions to silver element in AgNPs. The UV-Vis, FT-IR, SEM, EDX, XRD, zeta nanosizer, and zeta potential techniques-based characterization confirmed the formation of LTEO-AgNPs and high stability on their storage at room temperature. UV-Vis measurement showed the characteristic peak of synthesized AgNPs at 420 nm. FT-IR analysis displayed the functional groups involved in the synthesis of AgNPs as the bioreducing, capping, and stabilizing agents. SEM profile exhibited the synthesized AgNPs with the predominantly spherical shape and average size of 89.59 ± 5.14 nm (diameter). EDX peak indicated the existence of Ag element in LTEO-AgNPs. XRD analysis demonstrated LTEO-AgNPs possess crystalline property with the face-centered cubic structure. Zeta potential measurement displayed LTEO-AgNPs were highly stable in the colloidal suspension. The storage stability tests for the synthesized AgNPs showed stronger stability for the longer period of time at room temperature than in refrigerator. The evaluation of various concentrations of LTEO-AgNPs solution demonstrated good antibacterial, seed germination and seedling growth enhancing, colorimetric probe of metal ions, and catalytic activities. This research is the first report on AgNPs synthesis and evaluating their potential application for this specific plant species. However, even though AgNPs were reported to have wide applications in the various fields, only limited numbers of activities were reported in this study. Therefore, in

the future, further research efforts will be required to investigate all the potential activities of LTEO-AgNPs in large scale in the various areas of applications.

Author Contributions: Conceptualization, Y.H.G.; Formal analysis, Y.H.G.; Funding acquisition, P.K.; Investigation, Y.H.G.; Methodology, Y.H.G.; Software: Y.H.G.; Project administration: S.M.W. and K.A.D.; Resources: S.M.W.; Supervision, M.G.T. and R.K.B.; Validation, A.A.G., B.H., S.A.K., G.A.W., F.B.T., M.G.T., S.M.W., K.A.D., S.A.F., P.K., B.A., A.B. and R.K.B.; Visualization, A.A.G., B.H., S.A.K., G.A.W., F.B.T., A.B., M.G.T., S.M.W., K.A.D., S.A.F., P.K., B.A., A.B. and R.K.B.; Writing—original draft, Y.H.G.; Writing—review and editing, F.B.T., M.G.T., S.M.W., K.A.D., S.A.F., P.K., B.A., A.B. and R.K.B.; Characterization—SEM-EDX of LTEO-AgNPs, B.H., S.A.K., G.A.W.; Antibacterial activity evaluation, Y.H.G. and A.A.G. All authors have read and agreed to the published version of the manuscript.

Funding: This work was funded by the Researchers Supporting Project Number (RSP-2021/388) King Saud University, Riyadh, Saudi Arabia.

Institutional Review Board Statement: Not applicable.

Informed Consent Statement: Not applicable.

Data Availability Statement: Not applicable.

Acknowledgments: This work was funded by the Researchers Supporting Project Number (RSP-2021/388) King Saud University, Riyadh, Saudi Arabia. The authors acknowledge the helpful assistance from Central Research Laboratories of Addis Ababa Science & Technology University for providing instruments for spectroscopic analysis. We thank Cadila Pharmaceuticals Plc. (Ethiopia) for providing drug standards for antibacterial activity studies. Finally, we are grateful to the Laboratory Center for Traditional medicinal Plants, Ethiopian Public Health Institute, Addis Ababa, for their cooperation in providing all facilities for the antibacterial activities of essential oils and their silver nanoparticles.

Conflicts of Interest: The authors declare no conflict of interest.

References

1. Singh, J.; Dutta, T.; Kim, K.H.; Rawat, M.; Samddar, P.; Kumar, P. Green synthesis of metals and their oxide nanoparticles: Applications for environmental remediation. *J. Nanobiotechnol.* **2018**, *16*, 84. [CrossRef] [PubMed]
2. Balashanmugam, P.; Kalaichelvan, P.T. Biosynthesis characterization of silver nanoparticles using *Cassia roxburghii* DC. aqueous extract, and coated on cotton cloth for effective antibacterial activity. *Int. J. Nanomed.* **2015**, *10*, 87–97. [CrossRef] [PubMed]
3. Khandel, P.; Yadaw, R.K.; Soni, D.K.; Kanwar, L.; Shahi, S.K. Biogenesis of metal nanoparticles and their pharmacological applications: Present status and application prospects. *J. Nanostruc. Chem.* **2018**, *8*, 217–254. [CrossRef]
4. Pantidos, N.; Horsfall, L.E. Biological synthesis of metallic nanoparticles by bacteria, fungi and plants. *J. Nanomed. Nanotechnol.* **2014**, *5*, 1000233. [CrossRef]
5. Habibullah, G.; Viktorova, J.; Ruml, T. Current strategies for noble metal nanoparticle synthesis. *Nanosc. Res. Lett.* **2021**, *16*, 47. [CrossRef]
6. Rashmi, V.; Prabhushankar, H.B.; Sanjay, K.R. *Centella asiatica* L. callus mediated biosynthesis of silver nanoparticles, optimization using central composite design, and study on their antioxidant activity. *Plant Cell Tissue Org. Cult.* **2021**, *146*, 515–529. [CrossRef]
7. Bhumi, G.; Linga, R.M.; Savithramma, N. Green synthesis of silver nanoparticles from the leaf extract of *Adhatoda vasica* nees and assessment of its antibacterial activity. *Asian J. Pharm. Clin. Res.* **2015**, *8*, 62–67.
8. Kumar, B. Green synthesis of gold, silver, and iron nanoparticles for the degradation of organic pollutants in wastewater. *J. Compos. Sci.* **2021**, *5*, 219. [CrossRef]
9. Saeed, S.A. Silver nanoparticles (AgNPs) from plant extracts. *Life App. Sci.* **2019**, *70*, 70–95. [CrossRef]
10. Sana, S.S.; Li, H.; Zhang, Z.; Sharma, M.; Usmani, Z.; Hou, T.; Netala, V.R.; Wang, X.; Gupta, V.K. Recent advances in essential oils-based metal nanoparticles: A review on recent developments and biopharmaceutical applications. *J. Mol. Liq.* **2021**, *333*, 115951. [CrossRef]
11. De Oliveira Brisola Maciel, M.V.; da Rosa Almeida, A.; Machado, M.H.; Elias, W.C.; da Rosa, C.G.; Teixeira, G.L.; Noronha, C.M.; Bertoldi, F.C.; Nunes, M.R.; de Armas, R.D.; et al. Green synthesis, characteristics and antimicrobial activity of silver nanoparticles mediated by essential oils as reducing agents. *Biocatal. Agric. Biotechnol.* **2020**, *28*, 101746. [CrossRef]
12. Pryshchepa, O. Silver nanoparticles: Synthesis, investigation techniques, and properties. *Adv. Colloid. Interface Sci.* **2020**, *284*, 87–100. [CrossRef] [PubMed]
13. Salayová, A.; Bedlovičová, Z.; Daneu, N. Green synthesis of silver nanoparticles with antibacterial activity using various medicinal plant extracts: Morphology and antibacterial efficacy. *Nanomaterials* **2021**, *11*, 1005. [CrossRef] [PubMed]

14. Tarannum, N.; Divya, G.Y.K. Facile green synthesis and applications of silver nanoparticles: A state-of-the-art review. *RSC Adv.* **2019**, *9*, 34926–34948. [CrossRef]
15. Sharifi-Rad, M.; Pohl, P.; Epifano, F. Phytofabrication of silver nanoparticles (AgNPs) with pharmaceutical capabilities using *Otostegia persica* (burm.) boiss. leaf extract. *Nanomaterials* **2021**, *11*, 1045. [CrossRef]
16. Bhardwaj, K.; Dhanjal, D.S.; Sharma, A.; Nepovimova, E.; Kalia, A.; Thakur, S.; Bhardwaj, S.; Chopra, C.; Singh, R.; Verma, R.; et al. Conifer-derived metallic nanoparticles: Green synthesis and biological applications. *Int. J. Mol. Sci.* **2020**, *21*, 9028. [CrossRef]
17. Ahmed, A.A.Q.; Xiao, L.; McKay, T.J.M.; Yang, G. Green Metal-Based Nanoparticles Synthesized Using Medicinal Plants and Plant Phytochemicals against Multidrug-Resistant Staphylococcus aureus. In *Green Synthesis in Nanomedicine and Human Health*; CRC Press: Boca Raton, FL, USA, 2021; pp. 181–246.
18. Vilas, V.; Philip, D.; Mathew, J. Biosynthesis of Au and Au/Ag alloy nanoparticles using *Coleus aromaticus* essential oil and evaluation of their catalytic, antibacterial and antiradical activities. *J. Mol. Liq.* **2016**, *221*, 179–189. [CrossRef]
19. Sepahvand, R.; Delfan, B.; Ghanbarzadeh, S.; Rashidipour, M.; Veiskarami, G.H.; Ghasemian-Yadegari, J. Chemical composition, antioxidant activity and antibacterial effect of essential oil of the aerial parts of *Salvia sclareoides*. *Asian Pac. J. Trop. Med.* **2014**, *7*, 491–496. [CrossRef]
20. Bampouli, A.; Kyriakopoulou, K.; Papaefstathiou, G.; Louli, V.; Krokida, M.; Magoulas, K. Comparison of different extraction methods of *Pistacia lentiscus* var. chia leaves: Yield, antioxidant activity and essential oil chemical composition. *J. App. Res. Med. Aromat. Plants* **2014**, *1*, 81–91. [CrossRef]
21. Abdellatif, F.; Hassani, A. Chemical composition of the essential oils from leaves of *Melissa officinalis* extracted by hydrodistillation, steam distillation, organic solvent, and microwave hydrodistillation. *J. Mater. Environ. Sci.* **2015**, *6*, 207–213.
22. Chamorro, E.R.; Zambón, S.N.; Morales, W.G.; Sequeira, A.F.; Velasco, G.A. Study of the chemical composition of essential oils by gas chromatography. In *Gas Chromatography in Plant Science, Wine Technology, Toxicology and Some Specific Applications*; IntechOpen: London, UK, 2012; pp. 307–324. [CrossRef]
23. Vasile, B.S.; Birca, A.C.; Musat, M.C.; Holban, A.M. Wound dressings coated with silver nanoparticles and essential oils for the management of wound infections. *Materials* **2020**, *13*, 1682. [CrossRef]
24. Mothana, R.A.; Alsaid, M.S.; Al-Musayei, N.M. Phytochemical analysis and in vitro antimicrobial and free-radical-scavenging activities of the essential oils from *Euryops arabicus* and *Laggera decurrens*. *Molecules* **2011**, *16*, 5149–5158. [CrossRef] [PubMed]
25. Lia, X.; Huoa, C.; Shi, Q.; Kiyota, H. Chemical constituents of the plants from the Genus *Laggera*. *Chem. Biobivers.* **2007**, *4*, 105–111. [CrossRef] [PubMed]
26. Omoregie, E.H.; Oluyemisi, K.F.; Koma, O.S.; Ibumeh, O.J. Chemical constituents of the essential oil of *Laggera pterodonta* (DC.) Sch. Bip. from North-Central Nigeria. *J. App. Pharm. Sci.* **2012**, *2*, 198–202. [CrossRef]
27. Gebreheiwot, K.; Amenu, D.; Asfaw, N. Cuathemone sesquiterpenes and flavones from *Laggera tomentosa* endemic to Ethiopia. *Bull. Chem. Soc. Ethiop.* **2010**, *24*, 267–271. [CrossRef]
28. Asfaw, N.; Storesund, H.J.; Aasen, A.J. Constituents of the essential oil of *Laggera* constituents of the essential oil of *Laggera tomentosa* Sch. Bip. ex Oliv. et Hiern endemic to Ethiopia. *J. Essent. Oil Res.* **2011**, *15*, 102–105. [CrossRef]
29. Yilma, H.G.; Fekade, B.T.; Abiy, A.G.; Sileshi, D.G.; Mesfin, G.T.; Archana, B.; Rakesh, K.B. Chemical compositions of essential oil from aerial parts of *Cyclospermum leptophyllum* and its application as antibacterial activity against some food spoilage bacteria. *J. Chem.* **2022**, *2022*, 5426050. [CrossRef]
30. Getahun, T.; Sharma, V.; Kumar, D.; Gupta, N. Chemical composition, and antibacterial and antioxidant activities of essential oils from *Laggera tomentosa* Sch. Bip. ex Oliv. et Hiern (*Asteraceae*). *Turk. J. Chem.* **2020**, *44*, 1539–1548. [CrossRef] [PubMed]
31. Chahardoli, A.; Hajmomeni, P.; Ghowsi, M.; Qalekhani, F.; Shokoohinia, Y.; Fattahi, A. Optimization of quercetin-assisted silver nanoparticles synthesis and evaluation of their hemocompatibility, antioxidant, anti-inflammatory, and antibacterial effects. *Adv. Sci. News* **2021**, *2100075*, 2100075. [CrossRef] [PubMed]
32. Saha, N.; Trivedi, P.; Dutta, G.S. Surface plasmon resonance (SPR) based optimization of biosynthesis of silver nanoparticles from rhizome extract of *Curculigo orchioides* Gaertn. and its antioxidant potential. *J. Clust. Sci.* **2016**, *27*, 1893–1912. [CrossRef]
33. Kartini, K.; Alviani, A.; Anjarwati, D.; Fanany, A.F. Process optimization for green synthesis of silver nanoparticles using Indonesian medicinal plant extracts. *Processes* **2020**, *8*, 998. [CrossRef]
34. Haque, M.A.; Hossain, M.S.; Akanda, M.R.; Haque, A.; Naher, S. Procedure optimization of *Limonia acidissima* leaf extraction and silver nanoparticle synthesis for prominent antibacterial activity. *ChemistrySelect* **2019**, *4*, 14276–14280. [CrossRef]
35. Gul, A.R.; Shaheen, F.; Rafique, R.; Bal, J.; Waseem, S.; Park, T.J. Grass-mediated biogenic synthesis of silver nanoparticles and their drug delivery evaluation: A biocompatible anti-cancer therapy. *Chem. Eng. J.* **2021**, *407*, 127202. [CrossRef]
36. Budhani, S.; Egboluche, N.P.; Arslan, Z.; Yu, H.; Deng, H. Phytotoxic effect of silver nanoparticles on seed germination and growth of terrestrial plants. *J. Environ. Sci. Health—Part C* **2019**, *37*, 330–355. [CrossRef]
37. Kalam, A.; Al-Sehemi, A.G.; Alrumman, S. Colorimetric optical chemosensor of toxic metal ion (Hg^{2+}) and biological activity using green synthesized AgNPs. *Green Chem. Lett. Rev.* **2018**, *11*, 484–491. [CrossRef]
38. Li, P.; Wang, Y.; Huang, H.; Ma, S.; Yang, H.; Xu, Z.L. High efficient reduction of 4-nitrophenol and dye by filtration through AgNPs coated PAN-Si catalytic membrane. *Chemosphere* **2021**, *263*, 127995. [CrossRef] [PubMed]
39. Kapoor, S.; Sood, H.; Saxena, S.; Chaurasia, O.P. Green synthesis of silver nanoparticles using *Rhodiola imbricata* and *Withania somnifera* root extract and their potential catalytic, antioxidant, cytotoxic, and growth-promoting activities. *Bioprocess Biosyst. Eng.* **2022**, *45*, 365–380. [CrossRef]

40. Ahmad, B.; Ali, J.; Bashir, S. Optimization and effects of different reaction conditions for the bioinspired synthesis of silver nanoparticles using *Hippophae rhamnoides* Linn. leaves aqueous extract. *World Appl. Sci. J.* **2013**, *22*, 836–843. [CrossRef]
41. Alzahrani, E.; Welham, K. Optimization preparation of the biosynthesis of silver nanoparticles using watermelon and study of its antibacterial activity. *Int. J. Basic Appl. Sci.* **2014**, *3*, 392. [CrossRef]
42. Arya, G.; Kumari, R.M.; Gupta, N.; Kumar, A.; Chandra, R.; Nimesh, S. Green synthesis of silver nanoparticles using *Prosopis juliflora* bark extract: Reaction optimization, antimicrobial and catalytic activities. *Artif. Cells Nanomed. Biotechnol.* **2018**, *46*, 985–993. [CrossRef]
43. Ahmed, F.; Kabir, H.; Xiong, H. Dual colorimetric sensor for Hg^{2+}/Pb^{2+} and an efficient catalyst based on silver nanoparticles mediating by the root extract of *Bistorta amplexicaulis*. *Front. Chem.* **2020**, *8*, 591958. [CrossRef]
44. Ramdath, S.; Mellem, J.; Mbatha, L.S. Anticancer and antimicrobial activity evaluation of cowpea-porous-starch-formulated silver nanoparticles. *J. Nanotechnol.* **2021**, *2021*, 5525690. [CrossRef]
45. Nomura, K.; Terwilliger, P.; Roy, K.; Srivastwa, A.K.; Ghosh, C.K. Anticoagulant, thrombolytic, and antibacterial activities of *Euphorbia acruensis* latex-mediated bioengineered silver nanoparticles. *Green Process. Synth.* **2019**, *8*, 590–599.
46. Vijayakumar, S.; Malaikozhundan, B.; Parthasarathy, A.; Saravanakumar, K.; Wang, M.H.; Vaseeharan, B. Nano biomedical potential of biopolymer chitosan-capped silver nanoparticles with special reference to antibacterial, antibiofilm, anticoagulant, and wound dressing material. *J. Clust. Sci.* **2020**, *31*, 355–366. [CrossRef]
47. Pontes-Quero, G.M.; Benito-Garzón, L.; Pérez Cano, J.; Aguilar, M.R.; Vázquez-Lasa, B. Amphiphilic polymeric nanoparticles encapsulating curcumin: Antioxidant, anti-inflammatory, and biocompatibility studies. *Mater. Sci. Eng. C* **2021**, *121*, 111793. [CrossRef] [PubMed]
48. Quintero-Quiroz, C.; Acevedo, N.; Zapata-Giraldo, J. Optimization of silver nanoparticle synthesis by chemical reduction and evaluation of its antimicrobial and toxic activity. *Biomater. Res.* **2019**, *23*, 27. [CrossRef] [PubMed]
49. Li, C.; Chen, D.; Xiao, H. Green synthesis of silver nanoparticles using *Pyrus betulifolia* Bunge and their antibacterial and antioxidant activity. *Mater. Today Commun.* **2021**, *26*, 102–108. [CrossRef]
50. Tsegay, M.G.; Gebretinsae, H.G.; Sackey, J.; Maaza, M.; Nuru, Z.Y. Green synthesis of khat mediated silver nanoparticles for efficient detection of mercury ions. *Mater. Today: Proc.* **2021**, *36*, 368–373. [CrossRef]
51. Agnihotri, S.; Sillu, D.; Sharma, G.; Arya, R.K. Photocatalytic and antibacterial potential of silver nanoparticles derived from pineapple waste: Process optimization and modeling kinetics for dye removal. *Appl. Nanosci.* **2018**, *8*, 2077–2092. [CrossRef]
52. Jain, S.; Mehata, M.S. Medicinal plant leaf extract and pure flavonoid mediated green synthesis of silver nanoparticles and their enhanced antibacterial property. *Sci. Rep.* **2017**, *7*, 15867. [CrossRef]
53. Sang, S.; Li, D.; Zhang, H. Facile synthesis of AgNPs on reduced graphene oxide for highly sensitive simultaneous detection of heavy metal ions. *RSC Adv.* **2017**, *7*, 21618–21624. [CrossRef]
54. Ibrahim, H.M.; Zaghloul, S.; Hashem, M.; El-Shafei, A. A green approach to improve the antibacterial properties of cellulose-based fabrics using *Moringa oleifera* extract in the presence of silver nanoparticles. *Cellulose* **2021**, *28*, 549–564. [CrossRef]
55. Iqbal, M.; Raja, N.I.; Mashwani, Z.U.R.; Hussain, M.; Ejaz, M.; Yasmeen, F. Effect of silver nanoparticles on growth of wheat under heat stress. *Iran J. Sci. Technol. Trans A Sci.* **2019**, *43*, 387–395. [CrossRef]
56. Awada, M.A.; Hendib, A.A.; Ortashic, K.M.; Alzahranid, B.; Solimane, D.; Alanazid, A.; Alenazid, W.; Tahaf, R.M.; Ramadang, R.; El-Tohamyh, M.; et al. Biogenic synthesis of silver nanoparticles using *Trigonella foenum-graecum* seed extract: Characterization, photocatalytic, and antibacterial activities. *Sens. Actuator A* **2021**, *323*, 112670. [CrossRef]
57. Tufail, M.S. Silver nanoparticles and their applications: A comprehensive review. *Pure Appl. Biol.* **2021**, *11*, 315–330. [CrossRef]
58. Chitra, K. Effects of silver nanoparticles on seed germination and seedling growth of radish (*Raphanus sativus L.*). *J. Env. Sci. Toxicol. Food Technol.* **2017**, *11*, 604–608. [CrossRef]
59. Azimpanah, R.; Solati, Z.; Hashemi, M. Green synthesis of silver nanoparticles and their applications as colorimetric probe for determination of Fe^{3+} and Hg^{2+} ions. *IET Nanobiotechnol.* **2017**, *12*, 673–677. [CrossRef]
60. Chen, J.; Liu, Y.; Xiong, Y. *Konjac glucomannan* reduced-stabilized silver nanoparticles for mono-azo and di-azo contained wastewater treatment. *Inorg. Chim. Acta* **2021**, *515*, 120058. [CrossRef]
61. Albukhari, S.M.; Ismail, M.; Akhtar, K.; Danish, E.Y. Catalytic reduction of nitrophenols and dyes using silver nanoparticles @cellulose polymer paper for the resolution of wastewater treatment challenges. *Colloids Surf. A Physicochem. Eng. Asp.* **2019**, *577*, 548–561. [CrossRef]
62. Yang, W.; Hu, W.; Zhang, J. Tannic acid/Fe^{3+} functionalized magnetic graphene oxide nanocomposite with high loading of silver nanoparticles as ultra-efficient catalyst and disinfectant for wastewater treatment. *J. Chem. Eng.* **2021**, *405*, 126629. [CrossRef]
63. Horta-Fraijo, P.; Smolentseva, E.; Simakov, A.; José-Yacaman, M.; Acosta, B. Ag nanoparticles in A4 zeolite as efficient catalysts for the 4-nitrophenol reduction. *Microporous Mesoporous Mater.* **2021**, *312*, 110707. [CrossRef]
64. Ismail, M.; Khan, M.I.; Khan, S.B.; Akhtar, K.; Khan, M.A.; Asiri, A.M. Catalytic reduction of picric acid, nitrophenols, and organic azo dyes via green synthesized plant supported Ag nanoparticles. *J. Mol. Liq.* **2018**, *268*, 87–101. [CrossRef]